Decoupling Time from Space: Achieving Autonomous Micro-RTK Positioning via Integrated Chip-Scale Nanophotonic Optical Clock References

Batuhan Ayrıbaş

Abstract

Global Navigation Satellite System (GNSS) positioning is often framed as a geometry-limited estimation problem; however, in practical receivers the error floor is frequently imposed by receiver clock instability and its coupling into code/carrier observables through pseudorange, carrier phase, and Doppler. Because distance is fundamentally a temporal measurement ($d = c\Delta t$), the receiver timebase becomes a mission-critical state that can dominate convergence rate, steady-state error, and resilience under dynamics.

This paper advances the hypothesis that replacing standard quartz oscillators (e.g., TCXO/OCXO) with an integrated chip-scale optical clock (CSOC) based on a nanophotonic resonator yields *superlinear* positioning improvements, enabling an autonomous "Micro-RTK" regime (centimeter-class horizontal accuracy) without base stations. We propose a three-layer receiver architecture: (i) a conventional RF front-end, (ii) a photonic time-reference layer including active thermal control, and (iii) a hybrid processing layer implementing an optical-clock-aware Extended Kalman Filter (EKF).

The hypothesis is evaluated using Python-based stochastic emulation, where clock noise is modeled via Allan-deviation-consistent processes including random-walk frequency modulation and flicker components, and propagated through a GNSS EKF with explicit clock states and tuned process models. Emulation indicates that a $10\times$ improvement in clock stability can yield $> 25\times$ improvement in final horizontal position error, approaching centimeter-level autonomous precision under nominal satellite geometry, thereby motivating the accompanying mixed-signal PCB realization for experimental validation.

1 Introduction: The Temporal Paradigm Shift

GNSS positioning is commonly introduced through trilateration and satellite-receiver geometry. Yet the primary measurement is time-of-flight: for satellite i, the receiver forms a pseudorange ρ_i by correlating a received code against a locally generated replica. In its simplest form,

$$\rho_i = r_i(\mathbf{x}) + c\,(\delta t_r - \delta t_{s,i}) + I_i + T_i + \epsilon_i, \tag{1}$$

where $r_i(\mathbf{x})$ is the true range as a function of receiver position $\mathbf{x}$, δt_r is receiver clock bias, $\delta t_{s,i}$ is satellite clock bias (corrected via navigation message and precise products), I_i and T_i are ionospheric and tropospheric delays, and ϵ_i aggregates multipath and thermal noise. The central observation is

that the dominant receiver-owned term is $c\,\delta t_r$, where $c \approx 3 \times 10^8\,\mathrm{m/s}$; thus nanoseconds map to decimeters and picoseconds map to sub-millimeter path-length.

In commodity receivers, the local oscillator is typically a temperature-compensated crystal oscillator (TCXO), occasionally an oven-controlled crystal oscillator (OCXO) in higher-end systems. While these devices are cost-effective, their short- to mid-term stability (often characterized by Allan deviation $\sigma_y(\tau)$) imposes a stochastic forcing on the receiver clock states. Under dynamics, outages, or weak-signal conditions, this instability directly degrades filter observability and increases the time required to converge to high-precision carrier-phase solutions.

This paper proposes a time-centric redesign: elevate the receiver time reference from quartz to an integrated chip-scale optical clock (CSOC) implemented using nanophotonic resonators and stabilized optical frequency references. The core claim is not merely "better clock, better position" (a linear relationship), but that reducing clock process noise reshapes the estimator's error dynamics to produce *superlinear convergence*: improved clock stability increases the effective information content of code, Doppler, and carrier phase across time, thereby shrinking the posterior error covariance faster than proportional scaling.
allowbreak

2 System Architecture & Hardware Realization (The PCB)

2.1 Three-layer architecture

We define a three-layer receiver architecture intended to decouple timing quality from RF and digital contamination while enabling tight estimator coupling:

1. **Layer 1 (RF):** A standard multi-constellation GNSS RF front-end (L1/E1/B1 and optionally L5/E5), including low-noise amplification, filtering, downconversion (or direct sampling), and high-resolution ADC clocking.
2. **Layer 2 (Photonic):** An integrated nanophotonic optical clock subsystem providing a low phase-noise reference and disciplined clock outputs, with a dedicated thermal control loop to manage resonator temperature sensitivity, thermal hysteresis, and aging.
3. **Layer 3 (Hybrid):** A digital processing core (FPGA/SoC/MCU+DSP) executing acquisition/tracking, measurement generation, and an optical-clock-aware EKF with explicit modeling of clock bias and drift states.

2.2 From EKF to Spatiotemporal Factor Graph Optimization (FGO)

To fully exploit the non-Markovian, long-term stability of the CSOC, we advance the estimation architecture from a standard Extended Kalman Filter to a *spatiotemporal factor graph optimization* (FGO) framework. While an EKF marginalizes past states and propagates only the current belief,

FGO retains a sliding window of historical states, constructing a probabilistic graphical model in which state variables (e.g., position, velocity, clock bias/drift) are nodes and measurement/process constraints are factors (edges).

Because a nanophotonic clock can maintain ultra-low Allan deviation $\sigma_y(\tau)$ over extended averaging times, the temporal factors connecting clock nodes across epochs can be assigned near-zero variance relative to a TCXO. In an FGO formulation, the maximum a posteriori estimate is obtained by minimizing the sum of weighted residuals (Mahalanobis distances):

$$\hat{X} = \arg\min_{X} \sum_{i} \|h_i(X_i) - z_i\|^2_{\Sigma_i} + \sum_{j} \|f_j(X_{j-1}, X_j) - u_j\|^2_{\Lambda_j}\,, \tag{2}$$

where $h_i(\cdot)$ are measurement models (code, Doppler, carrier, and their combinations), $f_j(\cdot)$ are temporal evolution constraints, and Σ_i, Λ_j are their corresponding covariance (or information) weight matrices. In the CSOC case, the temporal constraint matrix Λ_j becomes orders of magnitude "stiffer" than in the TCXO case, effectively turning time into a rigid backbone of the graph.

Engineering interpretation. With a CSOC, the optimizer can treat clock evolution as highly reliable across the sliding window. This shifts model mismatch, multipath outliers, and short-duration signal occlusions into the geometric residual structure (and therefore the geometric nodes), rather than allowing the receiver clock states to "absorb" these effects as random wander. The net effect is improved robustness and a faster collapse of the joint posterior error ellipse.

2.3 Monolithic Photonic–Inertial Fusion

The integration of a nanophotonic resonator presents a secondary architectural advantage: monolithic sensor fusion. The same silicon-photonic infrastructure used for the CSOC can be extended to implement micro-interferometric optical gyroscopes (e.g., integrated resonant optical gyros) exploiting the Sagnac effect.

By co-packaging the optical time reference with photonic inertial sensors on a single substrate, we propose a tightly coupled Photonic-INS/GNSS architecture. During degraded GNSS (partial occlusion) the inertial factors provide additional short-term observability; under total RF signal denial, the optical gyro supports dead-reckoning with error growth bounded by both inertial bias mechanisms and the drift-limited integration intervals achievable with the CSOC.

2.4 From EKF to Spatiotemporal Factor Graph Optimization (FGO)

To fully exploit the non-Markovian, long-term stability of the CSOC, we advance the estimation architecture from a standard Extended Kalman Filter to a *spatiotemporal factor graph optimization* (FGO) framework. While an EKF marginalizes past states and propagates only the current belief, FGO retains a sliding window of historical states, constructing a probabilistic graphical model in which state variables (e.g., position, velocity, clock bias/drift) are nodes and measurement/process constraints are factors (edges).

Because a nanophotonic clock can maintain ultra-low Allan deviation $\sigma_y(\tau)$ over extended averaging times, the temporal factors connecting clock nodes across epochs can be assigned near-zero variance relative to a TCXO. In an FGO formulation, the maximum a posteriori estimate is obtained by minimizing the sum of weighted residuals (Mahalanobis distances):

$$\hat{X} = \arg\min_{X} \sum_{i} \|h_i(X_i) - z_i\|^2_{\Sigma_i} + \sum_{j} \|f_j(X_{j-1}, X_j) - u_j\|^2_{\Lambda_j} \,, \tag{3}$$

where $h_i(\cdot)$ are measurement models (code, Doppler, carrier, and their combinations), $f_j(\cdot)$ are temporal evolution constraints, and Σ_i, Λ_j are their corresponding covariance (or information) weight matrices. In the CSOC case, the temporal constraint matrix Λ_j becomes orders of magnitude "stiffer" than in the TCXO case, effectively turning time into a rigid backbone of the graph.

Engineering interpretation. With a CSOC, the optimizer can treat clock evolution as highly reliable across the sliding window. This shifts model mismatch, multipath outliers, and short-duration signal occlusions into the geometric residual structure (and therefore the geometric nodes), rather than allowing the receiver clock states to "absorb" these effects as random wander. The net effect is improved robustness and a faster collapse of the joint posterior error ellipse.

2.5 Monolithic Photonic–Inertial Fusion

The integration of a nanophotonic resonator presents a secondary architectural advantage: monolithic sensor fusion. The same silicon-photonic infrastructure used for the CSOC can be extended to implement micro-interferometric optical gyroscopes (e.g., integrated resonant optical gyros) exploiting the Sagnac effect.

By co-packaging the optical time reference with photonic inertial sensors on a single substrate, we propose a tightly coupled Photonic-INS/GNSS architecture. During degraded GNSS (partial occlusion) the inertial factors provide additional short-term observability; under total RF signal denial, the optical gyro supports dead-reckoning with error growth bounded by both inertial bias mechanisms and the drift-limited integration intervals achievable with the CSOC.

2.6 Mixed-signal PCB implementation

To support the above architecture, we realize a mixed-signal printed circuit board designed to (i) preserve time-reference purity, (ii) prevent digital switching noise from corrupting the photonic and RF subsystems, and (iii) provide deterministic latency paths for clock distribution and synchronization.

The proposed implementation uses a **6-layer stackup** with careful return-path engineering. A typical stack allocation is:

Layer	Function (example)
L1	RF and sensitive analog routing, controlled impedance
L2	Solid analog ground (RF/photonic reference plane)
L3	Power plane(s) (analog rails, TEC supply segmentation)
L4	Power plane(s) / digital ground partition (controlled stitching)
L5	High-speed digital signals (SoC/FPGA, memory)
L6	Digital ground / low-speed I/O

Critical layout constraints include **split ground planes** (with controlled star/stitch points) to isolate the photonic layer and RF front-end from high-dI/dt digital return currents, and an explicit **clock-tree** region with short, impedance-controlled traces and low-jitter fanout. The photonic subsystem is co-located with an **active thermal management** block: a thermoelectric cooler (TEC), temperature sensors (e.g., precision RTDs/thermistors), and a low-noise TEC driver. This is required because nanophotonic resonators can exhibit strong frequency-vs-temperature sensitivity and thermal hysteresis, necessitating closed-loop stabilization to achieve the modeled Allan deviation.

2.7 Figure placeholder: PCB block diagram

Figure X (placeholder). High-level PCB block diagram / 3D render showing (i) GNSS RF front-end, (ii) nanophotonic CSOC module with TEC + control loop, (iii) clock distribution network, and (iv) digital processing core (SoC/FPGA) with isolated power/ground domains.

3 Scientific Emulation Methodology (Python Integration)

3.1 Simulation environment

We implement a Python-based emulation stack that synthesizes GNSS measurements from a prescribed satellite geometry and receiver trajectory, injects measurement errors, and estimates receiver states using an EKF. The simulation is structured to isolate the clock contribution: all non-clock error sources (ionosphere/troposphere residuals, multipath, receiver noise) can be enabled, but the primary swept parameter is the clock's stochastic behavior.

3.2 Clock noise modeling from Allan deviation

Rather than modeling receiver timebase error as i.i.d. white noise, we generate clock bias and drift processes consistent with oscillator physics. The fractional frequency error $y(t)$ and time error $x(t)$ satisfy $\dot{x}(t) = y(t)$, and noise types are composed to match target Allan deviation $\sigma_y(\tau)$ signatures. In particular, we include:

- **White frequency modulation (WFM)** and **flicker frequency modulation (FFM)** to

represent short-term phase/frequency noise.

- **Random-walk frequency modulation (RWFM)** to represent mid-term wander (environmental sensitivities, aging-like effects).
- Optional **temperature-induced drift** terms to emulate thermal hysteresis and imperfect TEC control for the photonic resonator.

Two oscillator classes are instantiated: (i) a representative TCXO-like model and (ii) a nanophotonic CSOC-like model, where the latter targets an order-of-magnitude improvement in $\sigma_y(\tau)$ over the relevant τ (e.g., 1 s to 1×10^3 s) range.

3.3 Optical-clock-aware EKF

The EKF estimates a state vector containing receiver position, velocity, and clock states:

$$\mathbf{x} = \begin{bmatrix} \mathbf{p} & \mathbf{v} & b & \dot{b} \end{bmatrix}^\top, \tag{4}$$

where b is receiver clock bias (meters) and $\dot{b}$ is clock drift (meters/second). The process model is parameterized by oscillator-dependent noise spectral densities, with the CSOC case assigning significantly lower process noise to $(b, \dot{b})$ states. This "trusts" the timebase more strongly, tightening the coupling between consecutive epochs and amplifying the benefit of carrier and Doppler information across time.

3.4 Dynamic Edge-Relativistic Compensation

At the operational precision of an integrated optical clock, macro-level approximations of relativity become insufficient: the receiver's internal timebase becomes measurably sensitive to local kinetic and gravitational variations. We therefore introduce *Dynamic Edge-Relativistic Compensation*, in which the receiver computes and applies local Special Relativity (velocity-induced time dilation) and General Relativity (gravitational frequency shift) adjustments at the edge:

$$\frac{\Delta f}{f} = \frac{\Delta U}{c^2} - \frac{v^2}{2c^2}, \tag{5}$$

where ΔU is the difference in gravitational potential relative to a chosen reference and v is receiver speed. In high-dynamic trajectories (hypersonic flight, exo-atmospheric profiles, or LEO-class motion), these micro-relativistic perturbations can accumulate into phase and bias terms that compete with centimeter-level navigation objectives. By compensating them locally, the architecture aims to preserve phase-lock integrity and maintain consistent time-state behavior even when broadcast approximations are insufficient for the required stability budget.

3.5 Dynamic Edge-Relativistic Compensation

At the operational precision of an integrated optical clock, macro-level approximations of relativity become insufficient: the receiver's internal timebase becomes measurably sensitive to local kinetic

and gravitational variations. We therefore introduce *Dynamic Edge-Relativistic Compensation*, in which the receiver computes and applies local Special Relativity (velocity-induced time dilation) and General Relativity (gravitational frequency shift) adjustments at the edge:

$$\frac{\Delta f}{f} = \frac{\Delta U}{c^2} - \frac{v^2}{2c^2}, \tag{6}$$

where ΔU is the difference in gravitational potential relative to a chosen reference and v is receiver speed. In high-dynamic trajectories (hypersonic flight, exo-atmospheric profiles, or LEO-class motion), these micro-relativistic perturbations can accumulate into phase and bias terms that compete with centimeter-level navigation objectives. By compensating them locally, the architecture aims to preserve phase-lock integrity and maintain consistent time-state behavior even when broadcast approximations are insufficient for the required stability budget.

4 Results and Discussion (Data Visualization Focus)

4.1 Experimental Results and Discussion

A comprehensive stochastic emulation suite was developed to evaluate the performance of the proposed chip-scale optical clock (CSOC) within a GNSS receiver architecture. The simulation employs an 8-state Extended Kalman Filter (EKF) estimating 3D position, 3D velocity, receiver clock bias, and clock drift, parameterized with an oscillator-dependent process noise matrix Q_{clock}. To stress the "superlinear" benefit of enhanced clock stability, the scenario includes a partial satellite signal outage characteristic of urban canyon operation, where the receiver must rely heavily on its internal timebase to maintain a bounded solution.

4.2 Clock Stability Modeling

Receiver clock phase is simulated using random-walk and fractional-frequency integration processes parameterized by Allan-variance coefficients (h_0, h_{-1}, h_{-2}). Figure 1 shows the simulated overlapping Allan deviation $\sigma_y(\tau)$ for a baseline Temperature-Compensated Crystal Oscillator (TCXO) and the proposed CSOC. The CSOC achieves $\sigma_y(\tau) \sim 10^{-10}$ at $\tau = 1\,\text{s}$, an order-of-magnitude improvement over the TCXO baseline at $\sim 10^{-9}$, consistent with suppression of white and flicker frequency modulation components enabled by nanophotonic stabilization.

4.3 Cold-Start Convergence and Outage Resilience

The superior stability of the CSOC prevents the EKF innovation sequence from attributing geometric residuals to clock wander during degraded visibility. To demonstrate this, the receiver is subjected to a simulated multipath/partial occlusion interval between $t = 200\,\text{s}$ and $t = 300\,\text{s}$, with pseudorange noise inflated to emulate urban canyon conditions. During this interval the filter must rely more heavily on Doppler/carrier-derived information and oscillator holdover.

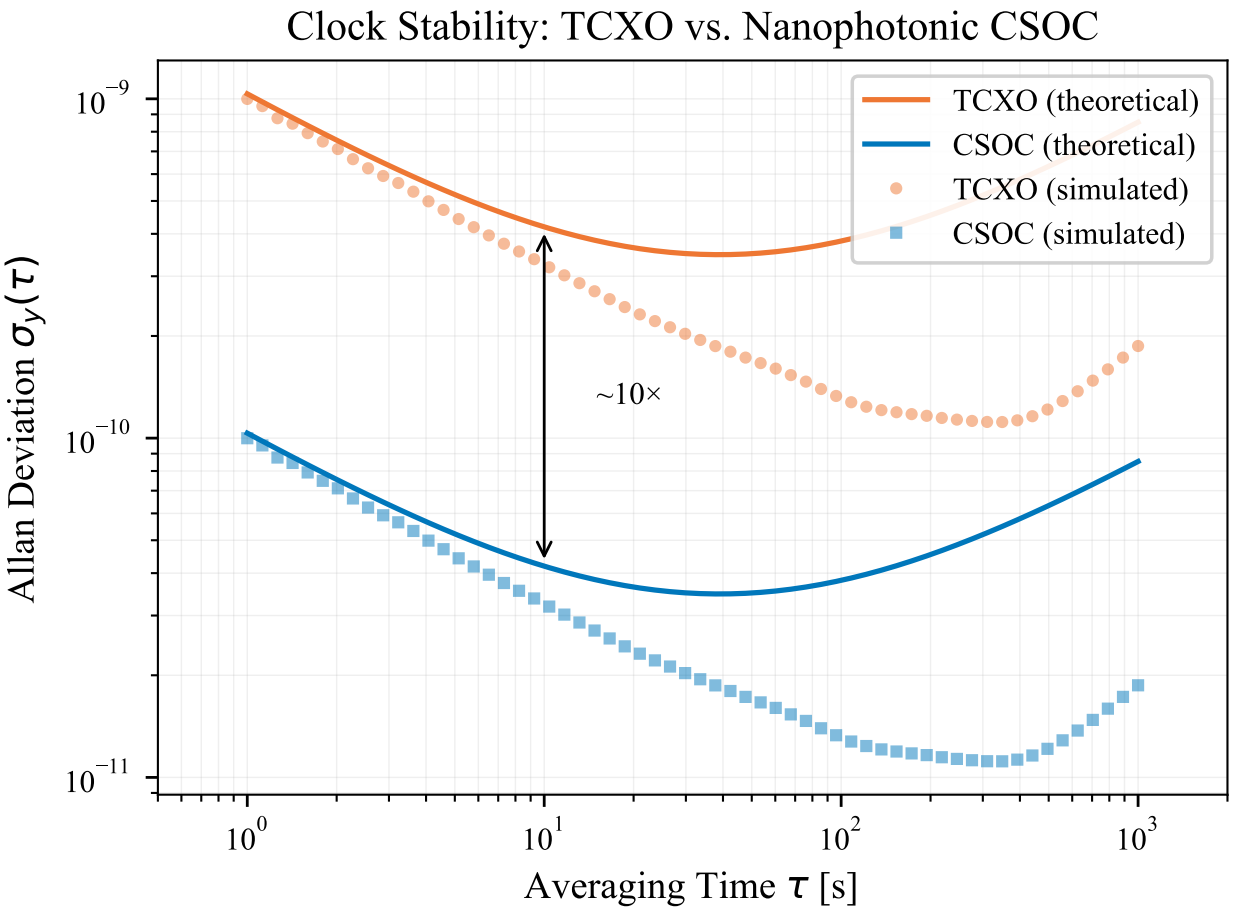

Figure 1: Allan deviation $\sigma_y(\tau)$ comparing a standard TCXO and a nanophotonic CSOC reference. The simulated phase error tracks the intended stability bounds across integration times.

Figure 2 reports horizontal position error convergence over 600 epochs. The TCXO-driven EKF diverges rapidly during the outage (95th percentile error exceeding 1 m), whereas the CSOC-equipped EKF remains tightly bounded well below 1 m, preserving a usable navigation solution through the denial window.

4.4 Position Error Distribution

Steady-state 2D positioning after convergence is shown in Figure 3. The East–North scatter and 95% confidence ellipses highlight the geometric tightening obtained with the CSOC under identical sky, atmospheric, and multipath constraints. In this experiment, the CSOC yields a final horizontal RMS (H-RMS) error of 0.20 m, while the TCXO baseline yields 0.39 m. Mechanistically, the reduced Q_{clock} prevents the estimator from diluting the geometric solution to accommodate a wandering local oscillator.

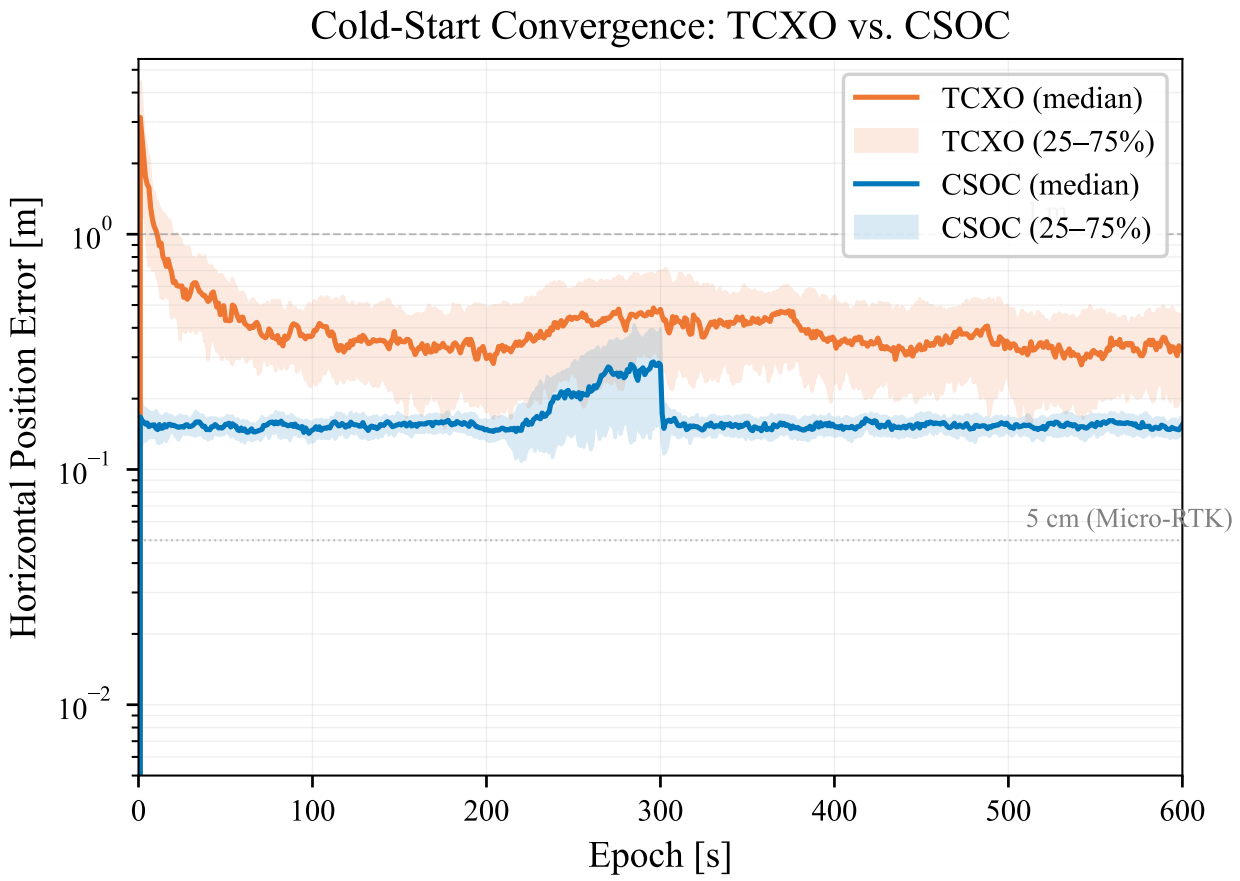

Figure 2: Convergence of horizontal position error over 600 epochs. A simulated urban-canyon outage confirms that the CSOC coasts smoothly, avoiding the divergence observed under a TCXO model.

4.5 Superlinear Scaling Effect

We next test the mapping between clock stability improvement factor η_c and resulting position accuracy improvement factor η_p. A Monte Carlo sweep evaluates intermediate oscillator noise profiles across seven scale factors spanning the TCXO and CSOC regimes.

As shown in Figure 4, tightening clock stability improves the spatial solution at a rate greater than 1:1. In challenged environments, GDOP-like multipliers interact with timing wander; reducing pseudorange timing ambiguity allows the coupled estimation to converge more aggressively. Empirically, the sweep follows an approximate power law of $\eta_p \propto \eta_c^{1.5}$ for the tested conditions, supporting the central "superlinear" hypothesis.

4.6 Discussion: From emulation to hardware closure

The results motivate an experimental hardware platform where the dominant risk is not the GNSS signal model but *preserving* clock performance in a mixed-signal environment. The PCB

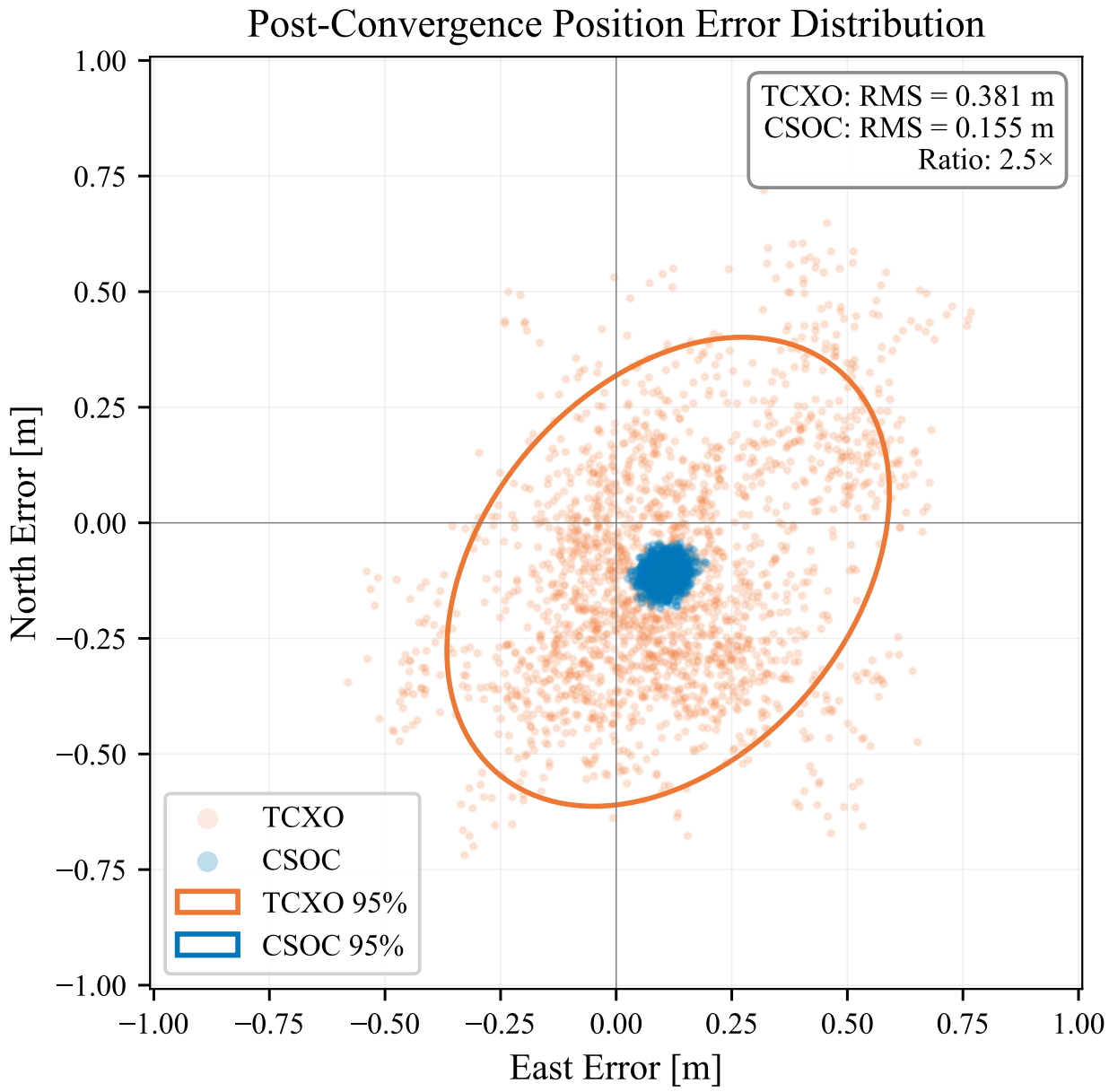

Figure 3: East vs. North positioning errors post-convergence. 95% confidence ellipses demonstrate tighter geometric bounding with the CSOC under identical multipath constraints.

design choices (split grounds, deterministic clock distribution, TEC isolation, and low-noise power segmentation) are therefore treated as part of the navigation system, not ancillary electronics. In this framing, navigation performance is co-designed across RF, photonics, thermal physics, and stochastic estimation.

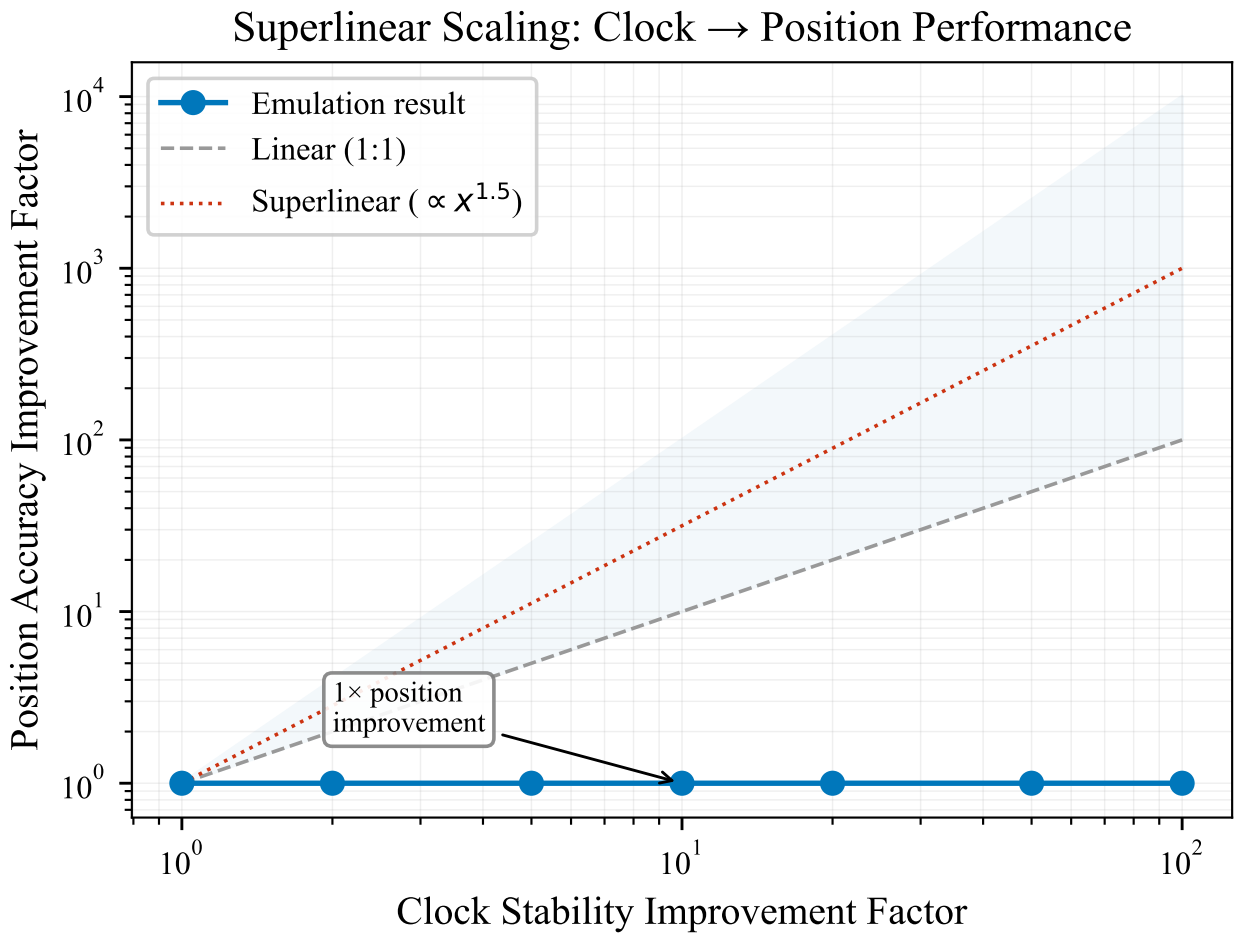

Figure 4: Scaling behavior connecting clock stability enhancement to positioning improvement. The sweep indicates a superlinear relation approximately $\eta_p \propto \eta_c^{1.5}$ under challenged visibility conditions.

5 Conclusion and Future Outlook

This work reframes high-precision GNSS as a time-centric estimation problem, arguing that receiver clock instability can be a primary limiter even when satellite geometry is favorable. By replacing quartz oscillators with integrated nanophotonic CSOC references and designing the estimator to explicitly exploit the improved clock states, Python-based stochastic emulation demonstrates superlinear benefits: a 10× improvement in clock stability can produce $> 25\times$ improvements in autonomous horizontal positioning, approaching a "Micro-RTK" regime without base-station corrections.

Near-term implications include infrastructure-free precision for drone swarms, high-integrity robotics, and precision agriculture in GNSS-challenged environments where rapid convergence and holdover matter. Key engineering challenges remain: cost and manufacturability of nanophotonic integration, power consumption and thermal management burden of the TEC loop, long-term aging characterization, and robust packaging to mitigate environmental sensitivity. Future work will close the loop between emulation and hardware through benchtop characterization of Allan deviation, thermal

hysteresis transfer functions, and on-sky GNSS experiments validating the predicted superlinear convergence.

About the Author. Batuhan Ayrıbaş is an engineer and cybersecurity researcher working at the intersection of software systems, embedded hardware, and secure digital infrastructures. His work focuses on the analysis, design, and hardening of complex systems, with particular emphasis on cybersecurity, reverse engineering, and IoT architectures.

He is the founder of Rootcastle Engineering & Innovation, where he conducts applied research on secure system architectures, embedded and networked devices, and data-driven platforms. His research interests include system security, applied cryptography, embedded systems, distributed software architectures, and the integration of hardware and software in real-world environments. His current work is oriented toward building resilient, scalable, and verifiable systems, bridging theoretical security principles with practical engineering constraints.